SUBVISIBLE RETINAL LASER THERAPY

Titration Algorithm and Tissue Response

DANIEL LAVINSKY, MD, PHD,*† CHRISTOPHER SRAMEK, PHD,‡ JENNY WANG, BSC,*
PHILIP HUIE, MSC,* ROOPA DALAL, MSC,* YOSSI MANDEL, MD, PHD,* DANIEL PALANKER, PHD*

Purpose: Laser therapy for diabetic macular edema and other retinal diseases has been used within a wide range of laser settings: from intense burns to nondamaging exposures. However, there has been no algorithm for laser dosimetry that could determine laser parameters yielding a predictable extent of tissue damage. This multimodal imaging and structural correlation study aimed to verify and calibrate a computational model–based titration algorithm for predictable laser dosimetry ranging from nondamaging to intense coagulative tissue effects.

Methods: Endpoint Management, an algorithm based on a computational model of retinal photothermal damage, was used to set laser parameters for various levels of tissue effect. The algorithm adjusts both power and pulse duration to vary the expected level of thermal damage at different percentages of a reference titration energy dose. Experimental verification was conducted in Dutch Belted rabbits using a PASCAL Streamline 577 laser system. Titration was performed by adjusting laser power to produce a barely visible lesion at 20 ms pulse duration, which is defined as the nominal (100%) energy level. Tissue effects were then determined for energy levels of 170, 120, 100, 75, 50, and 30% of the nominal energy at 1 hour and 3, 7, 30, and 60 days after treatment. In vivo imaging included fundus autofluorescence, fluorescein angiography, and spectral-domain optical coherence tomography. Morphologic changes in tissue were analyzed using light microscopy, as well as scanning and transmission electron microscopy.

Results: One hundred and seventy percent and 120% levels corresponded to moderate and light burns, respectively, with damage to retinal pigment epithelium, photoreceptors, and at highest settings, to the inner retina. 50% to 75% lesions were typically subvisible ophthalmoscopically but detectable with fluorescein angiography and optical coherence tomography. Histology in these lesions demonstrated some selective damage to retinal pigment epithelium and photoreceptors. The 30% to 50% lesions were invisible with in vivo multimodal imaging, and damage was limited primarily to retinal pigment epithelium, visible best with scanning electron microscopy. Over time, photoreceptors shifted into the coagulated zone, reestablishing normal retinal anatomy in lesions $\leq$100%, as seen in optical coherence tomography and light microscopy. Transmission electron microscopy at 2 months demonstrated restoration of synapses between shifted-in photoreceptors and bipolar cells in these lesions. Retinal pigment epithelium monolayer restored its continuity after 1 week in all lesions. No damage could be seen $<$30% level.

Conclusion: A retinal laser dosimetry protocol based on the Endpoint Management algorithm provides reproducible changes in retinal morphology in animals with various levels of pigmentation. This algorithm opens doors to clinical trials of well-defined subvisible and nondestructive regimes of retinal therapy, especially important for treatment of macular disorders.

RETINA 0:1–11, 2013

Retinal laser photocoagulation remains the standard of care, either alone or combined with pharmacological agents, for various retinal diseases, including proliferative diabetic retinopathy, diabetic macular edema (DME), vascular occlusions, central serous chorioretinopathy, and retinal tears. To minimize the side effects while retaining the therapeutic benefits, and to improve localization of the laser effects to specific retinal layers, various refinements in treatment parameters have been introduced, including variations in wavelength, pulse duration, and lesion intensity.

Introduction of the pattern scanning approach to retinal photocoagulation with the PASCAL photocoagulator in 2006[1] has advanced the use of shorter pulses

(10–30 ms), which limit heat diffusion, minimizing inner retinal damage and pain caused by reduced heating of the ciliary nerves in the choroid.[2,3] As a result, less damaging photocoagulation endpoints have been adopted,[4] which have been shown to decrease residual scarring and result in better restoration of the retinal structure and function.[5,6]

Selective and subvisible strategies have been developed to further minimize tissue damage, especially in the macula. These include selective retinal pigment epithelium therapy with microsecond pulses, which allow destruction of the retinal pigment epithelium (RPE) without damage to the photoreceptors and choroid.[7] During microsecond pulse, the heating is confined primarily to melanosomes, leading to explosive vaporization and associated destruction of RPE cells while avoiding damage to surrounding tissues. Retinal pigment epithelial cells proliferate and migrate from the surrounding areas, restoring complete coverage of the treated zone within a few days.[8] Clinical efficacy of selective RPE therapy has been demonstrated in applications to central serous chorioretinopathy and DME.[9]

A subvisible approach to retinal laser therapy was developed based on micropulse 810-nm diode laser, where power is titrated to the levels below clinically detectable tissue damage using relatively long (100–300 ms) bursts of 100 μs to 300 μs pulses. Randomized clinical trials have shown that subvisible treatment of DME delivered with high-laser spot density (<2 spot diameter spacing between burns) is equal or superior to the standard modified Early Treatment Diabetic Retinopathy Study protocol. However, the lack of a well-defined titration procedure is reflected in the variable results of these studies.[10–12]

Significant advantages of retinal phototherapy with a subvisible endpoint are the absence of scotomata and scarring, the ability to treat foveal areas, and improved preservation of color vision and contrast sensitivity.[13] The lack of chorioretinal damage permits high-density therapy, which greatly improves therapeutic outcomes compared with conventional sparse laser treatment protocols in the macula. Confluent laser applications can be safely delivered over the entire edematous areas, including retreatment of the same areas, even in the fovea.

However, the lack of a reliable titration protocol for reproducible subvisible treatment settings limits the clinical utility of this approach. If laser settings are too low, the treatment will be not only subvisible but also subtherapeutic, whereas if the settings are too high, there is a danger of excessive damage to the retina because of confluent coverage, especially in the fovea. The lack of a reproducible titration protocol for subvisible laser therapy inhibits its adoption in clinical practice.

As a step toward reproducible subvisible laser therapy, we developed a titration protocol based on Endpoint Management (EpM), a computational model–based algorithm for adjustment of laser power and duration. The titration protocol based on the EpM algorithm ties subvisible tissue effects to a visible titration point. To verify the protocol and define the ranges of the various tissue effects, we conducted a multimodal imaging and structural correlation study in rabbits using high-resolution optical coherence tomography (OCT), fluorescein angiography (FA), light microscopy (LM), transmission electron microscopy (TEM), and scanning electron microscopy (SEM).

Methods

Photocoagulation System

A PASCAL Streamline 577 (Topcon Medical Laser Systems, Inc., Santa Clara, CA) system provided 577-nm optical radiation from a diode-pumped solid state continuous laser coupled into a scanning system integrated with a slit lamp. In this system, the laser beam (flat–top profile) is projected onto the retina, and a graphic user interface allows control over laser parameters, including the spot size, power, and pulse duration. This system provided 10 ms to 100 ms pulses with up to 2 W power and an aerial spot size ranging from 100 μm to 400 μm.

Laser Application

A total of 8 Dutch-belted rabbits (16 eyes) were used in accordance with the Association for Research in Vision and Ophthalmology Resolution on the Use of Animals in Ophthalmic and Vision Research, with approval from the Stanford University Animal Institutional Review Board. All 16 eyes were submitted to multimodal imaging (OCT and FA): 6 eyes were used for SEM and the remaining 10 for either LM or TEM. The rabbits were anesthetized using ketamine hydrochloride (35 mg/kg), xylazine (5 mg/kg), and glycopyrrolate (0.01 mg/kg). Pupil dilation was achieved by 1 drop each of 1% tropicamide and 2.5% phenylephrine

From the *Department of Ophthalmology, Stanford University, Stanford, California; †Universidade Federal do Rio Grande do Sul, Hospital de Clinicas de Porto Alegre, Department of Ophthalmology, Porto Alegre, RS, Brazil; and ‡Topcon Medical Laser Systems, Inc., Santa Clara, California.

D. Palanker has a Stanford University patent on patterned scanning laser photocoagulation licensed to Topcon Medical Laser Systems with an associated royalty interest. D. Palanker and D. Lavinsky serve as consultants for Topcon Medical Laser Systems and C. Sramek is currently an employee at Topcon Medical Laser Systems.

Reprint requests: Daniel Lavinsky, MD, PhD, Department of Ophthalmology, Stanford University, 452 Lomita Mall, Stanford, CA 94305-4085; e-mail: daniellavinsky@gmail.com

hydrochloride. Topical tetracaine hydrochloride 0.5% was used for local anesthesia. A Mainster wide-field retinal contact lens (Ocular Instruments, Bellevue, WA) was used with hydroxypropyl methylcellulose as a contact gel. In a rabbit eye, this lens provides a retinal beam size that is equal to the aerial spot size.

Endpoint Management Algorithm

Laser power and duration parameters in this study followed the algorithm implemented in the EpM software package for PASCAL lasers (Topcon Medical Laser Systems). This software uses a computational model of retinal heating to provide a mapping between laser pulse energy and expected tissue effect. This model, developed to estimate retinal lesion size, approximated the retina as a series of homogeneous absorbing layers and coupled an axisymmetric heat conduction model with the Arrhenius cellular damage model.[14]

For pulse durations exceeding 50 μs, thermal denaturation of tissue has been shown to be the primary retinal damage mechanism.[15,16] In this regime, the damage can be described with first-order reaction kinetics (Arrhenius law) parameterized by an activation energy, corresponding to the denaturation of a single critical component and assuming an absence of cellular repair. The rate of decrease in concentration of the critical molecular component $D(t)$ is assumed to change with temperature $T(t)$:

$$dD(t) = -D(t) \cdot A \cdot \exp\left(-\frac{E^*}{R \cdot T(t)}\right)dt,$$

where E^* and A are the activation energy and rate constant parameterizing the process, and R is the gas constant (8.3 J/K·mol). Tissue damage, that is, decrease in critical molecular component $D(\tau)$ over the duration of hyperthermia τ, relative to its initial value D_0, is encapsulated in the Arrhenius integral Ω:

$$\Omega(\tau) = -\ln\left(\frac{D(\tau)}{D_0}\right) = A\int_0^{\tau} \exp\left(-\frac{E^*}{R \cdot T(t)}\right)dt.$$

The criterion for cell viability is then determined as a maximum tolerable decrease in concentration of the critical component; the Arrhenius integral is generally normalized to unity at this threshold ($\Omega = 1$).

Experiments with heat shock protein expression after nondamaging retinal exposures in mouse,[17] as well as a computational analysis of clinical laser settings[18] indicated that nondestructive thermal therapy corresponds to Arrhenius values approximately $\Omega = 0.1$ to 1.[17] Because of the exponential dependence of the integral on temperature, suprathreshold (visible) lesions have calculated values $\Omega >> 1$, and the relevant range for retinal thermal therapy spans several orders of magnitude. The EpM algorithm maps a range of calculated Arrhenius integral values to linear steps in pulse energy, normalized to a titration dose specified at a particular duration. Since the Arrhenius integral is a function of the pulse duration and laser power via the temperature time course $T(t)$, the mapping of a particular value of Ω to a fractional pulse energy uniquely defines a pulse duration and power.

Titration Protocol and In Vivo Imaging

Retinal treatment with the EpM algorithm using our protocol begins with titration of laser power to a minimally visible retinal lesion endpoint (the 100% EpM setting), and the laser pulse energy used during treatment is defined as a percentage of this titration energy. Each energy level corresponds to unique pair of laser power and pulse duration. For example, for 30, 50, and 75% energy levels (20 ms titration pulse duration), the pulse duration/fractional power is: 11.4 ms/52.8%, 15.9 ms/62.8%, and 18.7 ms/80.2%. As ophthalmoscopic lesion visibility changes over time (with lesions initially invisible often becoming visible after several minutes), lesion appearance must be evaluated at a consistent time point after laser delivery. For practical clinical usability, an evaluation time point of 3 seconds was defined for this protocol. Exposures with energy levels >100% were delivered with 20 ms duration, with the increase in energy corresponding to an increase in power alone. Pattern-scanned 2×5 treatment grids were applied at 30, 50, 75, 100, 120, and 170% levels, whereasthe intense marker burns were applied using 50 ms exposures. Spot sizes of 100, 200, and 400 μm were used. Treatment was applied in each eye at 1 hour, as well as 1, 3, 7, 30, and 60 days before euthanasia.

Retinal lesions were imaged in vivo during the follow-up period using FA, fundus autofluorescence, and OCT (HRA2-Spectralis; Heidelberg Engineering, Heidelberg, Germany).

Tissue Pathology

Light and transmission electron microscopy. After euthanasia, eyes were enucleated and fixed in 1.25% glutaraldehyde/1% paraformaldehyde in cacodylate buffer (pH 7.2) overnight at room temperature. The tissue was then postfixed in osmium tetroxide, dehydrated with a graded series of ethanol, and processed with propylene oxide. Tissue was embedded into epoxy resin (EMbed 812; Electron Microscopy Sciences, Port Washington, PA). One-micrometer sections for light microscopy or 100-nm sections for TEM were cut on

Table 1. Clinical and Histopathologic Findings of Different Endpoints

Clinical Grade		Intense			Light and Barely Visible			Subvisible			NDPS		
Energy, %			170			100–200			50–75			30	
Spot size, μm		100	200	400	100	200	400	100	200	400	100	200	400
Visibility	Ophthal	+	+	+	+	+	+	–	–	–	–	–	–
	OCT	FT	FT	FT	OPL	OPL	OPL	ONL	ONL	IS/OS*	—	—	—
	FA	+	+	+	+	+	+	+	+	–	–	–	–
	LM	FT	FT	FT	ONL	ONL	ONL	ONL	ONL	ONL*	—	—	—
	SEM	RPE	RPE	RPE	RPE	RPE	RPE	RPE	RPE	RPE	—	RPE*	RPE*

*Occasional.
FT, full thickness; IS/OS, inner/outer segment junction; NDPS, nondestructive photostimulation; ONL, outer nuclear layer; OPL, outer plexiform layer.

an ultramicrotome (Reichert-Jung Ultracut E; Leica, Deerfield, IL). Sections for light microscopy were stained with toluidine blue and photographed on a light microscope (Eclipse E1000; Nikon, Tokyo, Japan). Thin sections for electron microscopy were stained with uranyl acetate and lead citrate. Transmission electron micrographs were captured with a JEM-1400 (JEOL USA, Inc., Peabody, MA).

Scanning Electron Microscopy

For SEM, 6 eyes were enucleated rapidly and the anterior segment of the globe was incised and separated from the posterior part of the eyecup, and the retina was manually peeled from the RPE. The remaining sclera, choroid, and RPE were fixed in glutaraldehyde–paraformaldehyde fixative (1.25%/1% in 0.2 M sodium cacodylate buffer) at room temperature for 30 minutes. The tissue was then fixed for additional 18 hours at 4°C, rinsed in a buffer, and postfixed in 1% osmium tetroxide in 0.2 M sodium cacodylate, pH 7.4. The tissue was washed with distilled water, dehydrated in a series of ethanols, transferred to absolute ethanol, critical point dried, mounted on stubs, and plasma coated with gold/palladium (Denton Vacuum, Moorestown, NJ). Samples were imaged with a Hitachi S-34000N VP-SEM (Hitachi, Pleasanton, CA).

Statistical Analysis

The ED50 is the median effective dose or the laser settings required to produce the specific effect (e.g., visibility by clinical evaluation, FA, or OCT) in 50% of the measurements. ED50 threshold energy levels were calculated by Probit analysis in MATLAB (version 7.4; Mathworks, Inc., Natick, MA) separately for each eye.

Results

Table 1 summarizes the extent of tissue damage and visibility of the lesions in vivo and ex vivo for 100, 200, and 400 μm laser spot sizes. Figure 1 shows the 2 × 5 pattern of 30, 50, 75, 100, 120, and 170% nominal energy as well as marker burns. The same pattern was applied with 100, 200, and 400 μm spot sizes. Because of space constraints and highest clinical relevance, we focus below primarily on the description of the 200-μm data.

Ophthalmoscopically, only the burns of titration level (100%) and higher were visible within 3 seconds

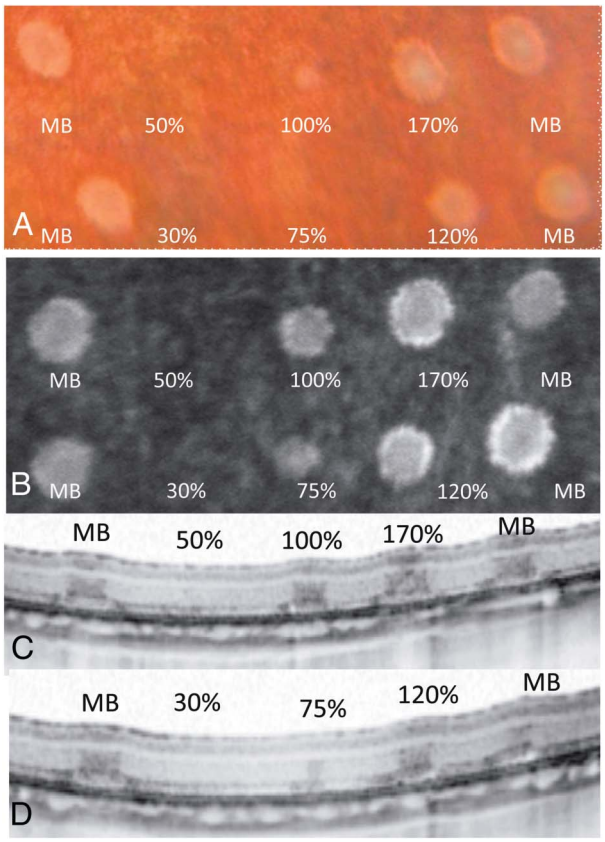

Fig. 1. A. Color fundus photograph of a dosimetry grid with 200 μm spot size, imaged 1 hour after laser treatment. Percentage indicates the energy setting of each lesion. **B.** Fluorescein angiography at 1 hour shows visible spots at energy levels exceeding 50%. **C** and **D.** Optical coherence tomography at 1 hour. Damage is clearly seen at energy levels exceeding 50% as dark areas in the photoreceptor layer. Only the intense marker burns (MB) and 170% burn caused inner retinal damage.

COLOR

of laser application. However, tissue effects at 75% and occasionally at 50% energy were identifiable with FA and OCT and ophthalmoscopically >3 seconds after laser application. In vivo imaging techniques did not show signs of tissue damage below the 50% level. Probability of retinal damage (Probit analysis) as a function of energy is plotted in Figure 2. The ED50 thresholds for ophthalmoscopic visibility, FA, and OCT were at 71, 64, and 54%, respectively. The 30% level had zero probability of retinal damage with all 3 in vivo criteria.

Moderate and Intense Burns (120–170%)

Intense (170%) burns caused full-thickness damage visible by OCT (Figure 1C). Light microscopy confirmed damage to the inner and outer retina and even the retinal nerve fiber layer. Scanning electron microscopy of the intense burns showed condensed vitreous attached to the surface of the retina and a break at the inner limiting membrane (Figure 3). Transmission electron microscopy revealed coagulation of nuclei and cytoplasm of most inner retinal cells, with complete destruction of the synapses in both plexiform layers. Damage in the light-to-moderate burns (120%) was limited to the photoreceptors layer and RPE (Figure 1C).

Barely Visible Burns (100%)

Per the titration protocol described above, 100% energy level was defined for retinal lesions ophthalmoscopically barely visible at 3 seconds after laser application. Barely visible burns were always visible in FA, whereas OCT demonstrated hyperreflective changes in the photoreceptor layer (Figure 1). Light microscopy at 1 hour demonstrated damaged inner and outer segments and pyknotic nuclei in the outer nuclear layer (Figure 4A). After 3 days, TEM showed an absence of photoreceptors in the middle of the burn with less damaged nuclei at the edges of the lesion and an absence of the synapses in the outer plexiform layer (Figure 5). Scanning electron microscopy of RPE 1 hour after the laser application showed damaged outer segments of photoreceptors attached to the damaged RPE underneath (Figure 4B). Two and 7 days later, the continuity of the RPE monolayer was progressively reestablished, with the damage zone covered by a mixture of large and small cells, both with microvilli on the apical surface, indicating presence of adjacent photoreceptors (Figure 4, C and D). Transmission electron microscopy also demonstrated reestablishment of basal infoldings in the RPE cells at the center of the burn at 7 days (data not shown).

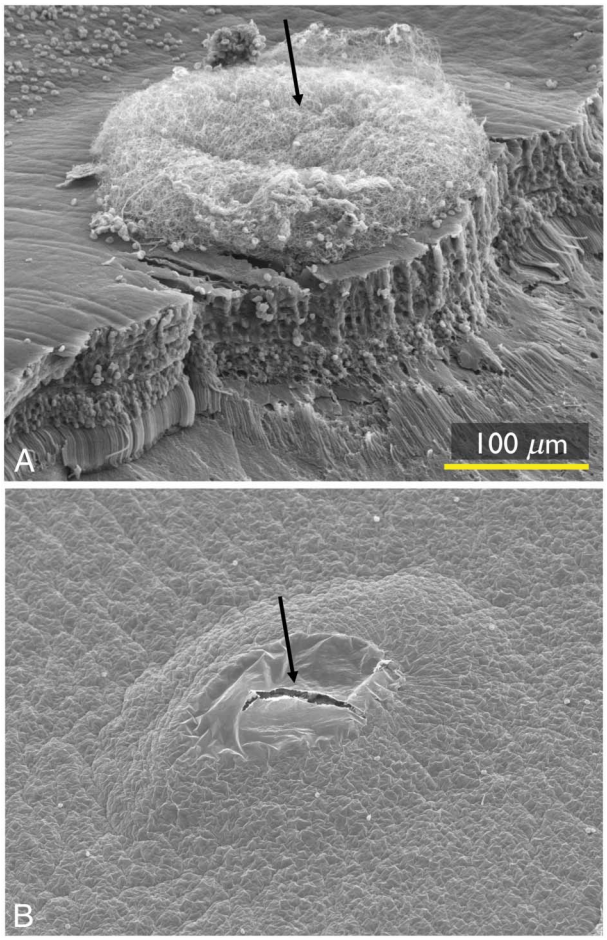

COLOR

Fig. 3. A. Scanning electron microscopy of an intense marker burn with condensed vitreous attached to the surface of the retina over the laser spot (arrow). Tissue layers are clearly seen at the edge of the retina to the right of the burn. **B.** Scanning electron microscopy of the retinal surface over an intense laser burn with a break at the inner limiting membrane (arrow).

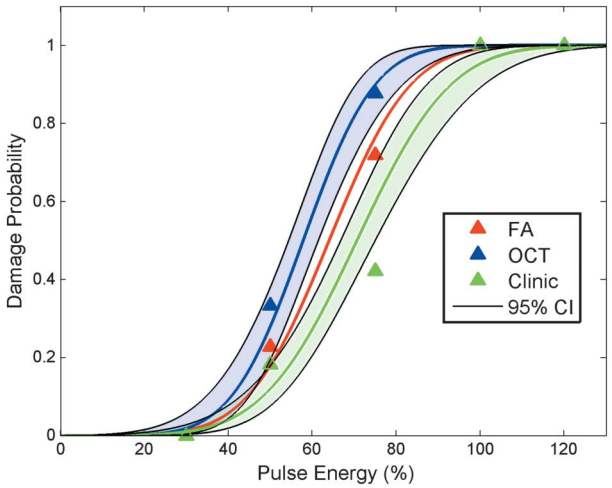

COLOR

Fig. 2. Probability of the retinal damage (Probit analysis) as a function of the energy settings, relative to the barely visible burn, defined as 100%. The damage visibility criteria include: ophthalmoscopic visibility, OCT, and FA. ED50 for FA is 64%, OCT is 58%, and ophthalmoscopic visibility is 71%.

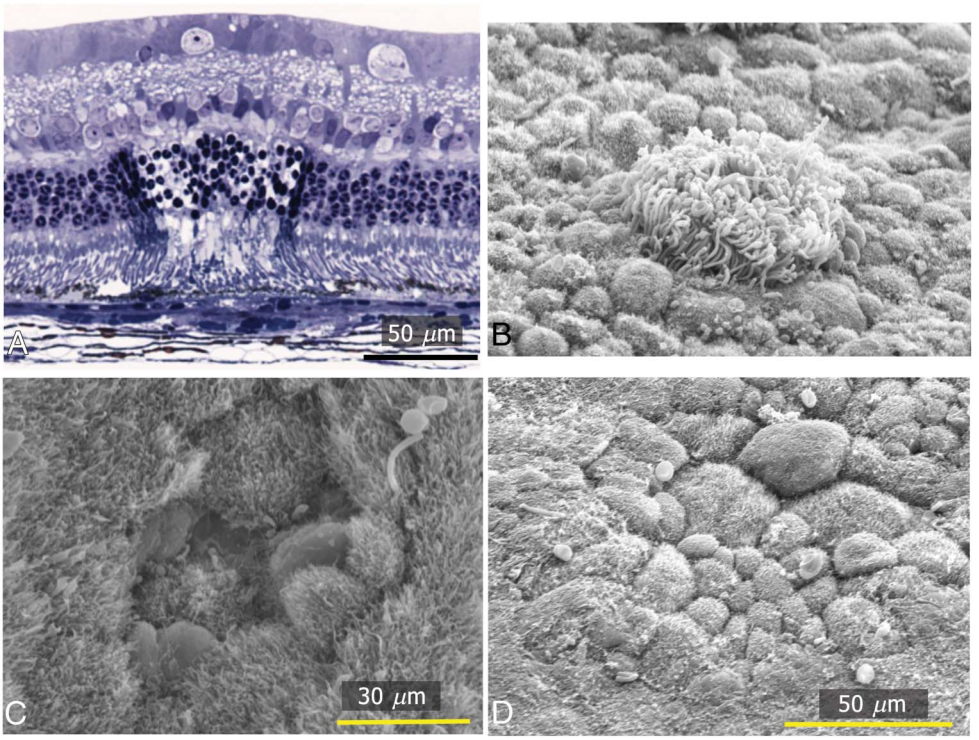

COLOR

Fig. 4. A. Light microscopy of a barely visible (100%) lesion at 1 hour. Spot size 200 μm. **B.** Scanning electron microscopy of RPE at 1 hour shows attached outer segments of photoreceptors. **C.** At 2 days, RPE cells from the periphery of the wound started migrating into the damage zone. **D.** At 7 days, continuity of the RPE monolayer is reestablished, with a damage zone covered by a mixture of large and small cells. Microvilli on the apical surface of the cells indicate the presence of photoreceptors above.

At 2 months, autofluorescence was enhanced in the marker burn, 170 and 100% burns, but not in the 50 or 30% sites (Figure 6A). Optical coherence tomography demonstrated recovery of the inner and outer segment junction line for most of the 100% burns after 2 months, and no signs of residual damage in the 50% lesions (Figure 6B). Light microscopy confirmed restoration of photoreceptor layer with slightly reduced nuclei density at the outer nuclear layer (Figure 6C). Transmission electron microscopy demonstrated reestablishment of the normal synaptic ribbons and vesicles at the center of the burn (Figure 6D). Scanning electron microscopy demonstrated continuous RPE monolayer in the former damage zone, with microvilli on the

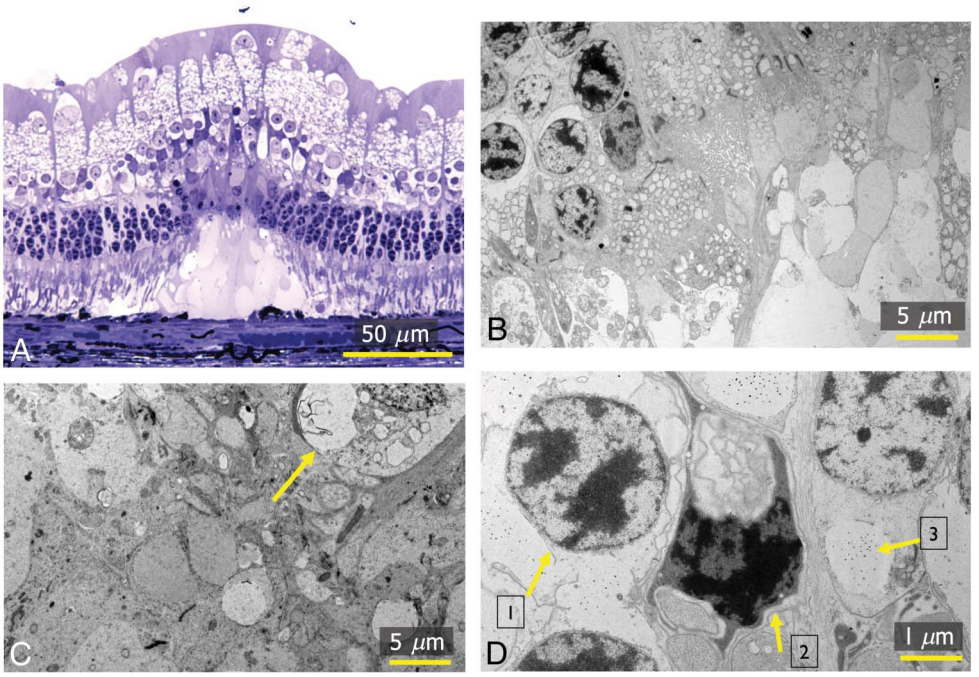

COLOR

Fig. 5. A. Light microscopy of a barely visible (100%) burn at 3 days. Spot size 200 μm. **B.** Transmission electron microscopy at 3 days shows absence of the photoreceptors' nuclei and their inner and outer segments in the middle of the lesion (right side of the image), with less damaged cells on the left edge of the burn. **C.** Transmission electron microscopy at 3 days shows absence of normal synapses in the outer plexiform layer between bipolar cells (arrow) and photoreceptors (absent). **D.** Transmission electron microscopy at the edge of the burn at 3 days shows normal nucleous (1), pyknotic nucleus (2) with damaged synaptic ribbon and depleted vesicles (3).

COLOR

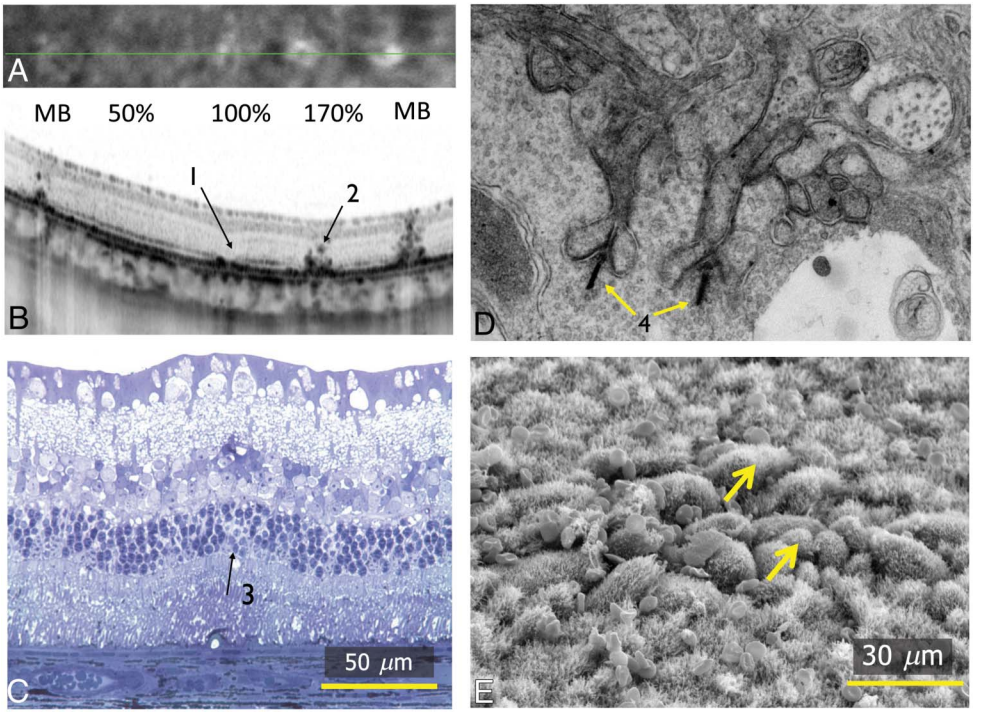

Fig. 6. A. Fluorescein angiography of a dosimetry grid with 200-μm spots at 2 months shows hyperfluorescence at the marker burn (MB), 170% and 100% burns, but no hyperfluorescence or hypofluorescence at 50% or 30% sites. **B.** Optical coherence tomography at 2 months shows partial recovery of the inner and outer segment junction line for 100% burn (1) and no damage at the 50% exposure. The 170% burn shows hyperreflective lesion (2) with disruption of inner/ outer segment line; however, no inner retinal damage is observed, unlike in the intense marker burn to the right. **C.** Light microscopy shows recovery of the photoreceptor layer with slightly reduced nuclei density (arrow) at the outer nuclear layer (3). **D.** Transmission electron microscopy demonstrates reestablishment of the normal synaptic ribbons (4) and vesicles (arrows) at the center of the burn. **E.** Scanning electron microscopy shows restoration of RPE monolayer with microvilli on the cell surface. Retinal pigment epithelial cells in the center of the lesion have variable sizes—large and small (arrows).

apical surface, indicating presence of adjacent photoreceptors (Figure 6E).

Subvisible Burns (50–75%)

Fifty percent to 75% lesions were not visible ophthalmoscopically, but OCT and FA demonstrated signs of damage. In OCT, the 75% burns, and occasionally the 50% lesions, exhibited a smaller vertical hyperreflective band in the photoreceptors layer (Figure 1D). Light microscopy of a 50% burn after 1 hour demonstrated pyknotic nuclei of the photoreceptors (Figure 7A). Damage zone in the RPE was

COLOR

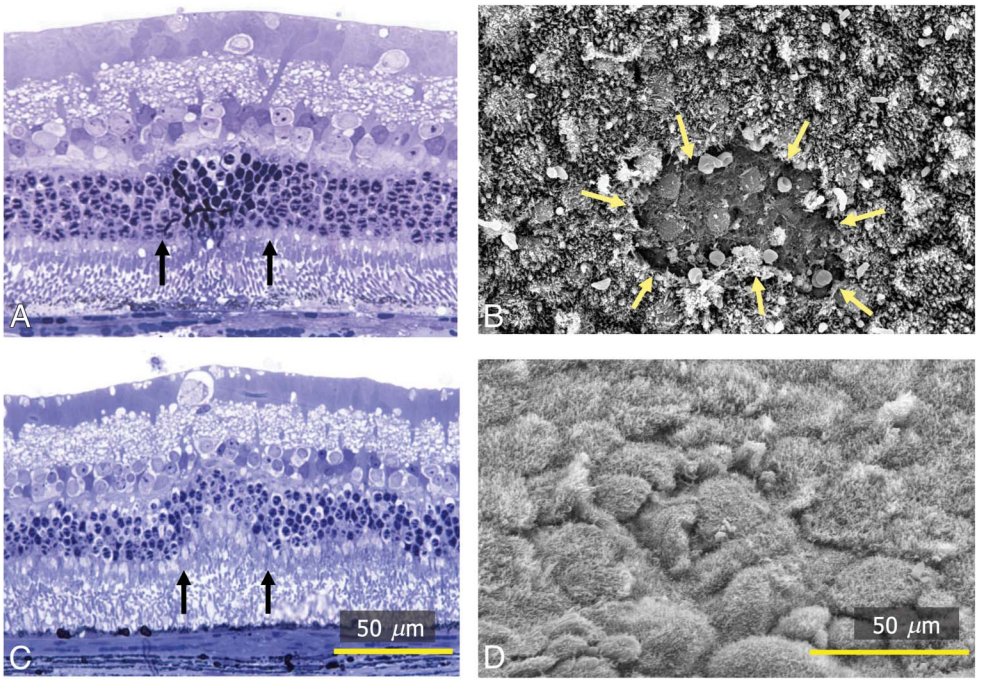

Fig. 7. A. Light microscopy of a 50% burn at 1 hour demonstrating pyknotic nuclei of photoreceptors (arrows). Spot size 200 μm. **B.** Scanning electron microscopy of RPE at 1 day shows limited damage in the center of the burn (arrows); however, surrounding cells seem to have normal morphology. **C.** Light microscopy at 3 days demonstrates partial loss of nuclei in the outer nuclear layer (arrows). **D.** Scanning electron microscopy at 3 days demonstrates recovery of the RPE monolayer in the former lesion.

decreased compared with 100% lesions, as seen in SEM (Figure 7B). At 3 days, LM demonstrated partial loss of photoreceptors nuclei, but there was no complete gap at the outer nuclear layer (Figure 7C). Scanning electron microscopy at 3 days demonstrated restoration of RPE monolayer in the burn (Figure 7D).

Nondamaging Photostimulation (30%)

The 30% exposures were not visible by any in vivo techniques. Light microscopy did not show any visible damage in the RPE or retina (Figure 8A), and TEM demonstrated normal RPE cells in the center of the exposure (Figure 8C) and normal synapses in the outer plexiform layer (Figure 8D), although occasional displaced RPE cells with phagosomes of the outer segments at the center of the laser spot could be identified (Figure 8B). Scanning electron microscopy at 1 day consistently identified a single damaged RPE cell in the center of the treatment area (Figure 9, A and B). However, after 7 days, there were no visible signs of damage to RPE layer in the irradiated spot (Figure 9, C and D).

Discussion

The working mechanism of retinal phototherapy is an area of active research. The pathophysiology underlying a number of retinal vascular disorders has implicated inflammation and hypoxia. These conditions induce angiogenic factors, such as vascular endothelial growth factor or inflammatory cytokines, that stimulate neovascularization or vascular permeability.[19,20] Thus, it has been traditionally thought that the destruction of the numerous metabolically demanding photoreceptors in poorly perfused portions of the retina during photocoagulation limits the ischemia and decreases the production of angiogenic factors.[13,21] Initially, laser applications commonly involved moderate and even intense burns (Early Treatment Diabetic Retinopathy Study), which would cause full-thickness retinal damage, including not only photoreceptors but also the inner retina and even the nerve fiber layer, leading to excessive visual field impairment and retinal atrophy.[22] As we have shown, intense burns can even rupture the internal limiting membrane and coagulate the vitreous, and this should be taken into account if one would consider using intense burns clinically. More recently, lighter lesions, limited to the photoreceptors and RPE layer have become more common,[23] especially upon introduction of the pattern scanning photocoagulation with pulse durations in the range of 20 to 30 ms.[1]

Although these working mechanisms have been generally accepted for treatment of proliferative diabetic retinopathy, alternative hypotheses have been suggested for macular therapy. It was assumed that the

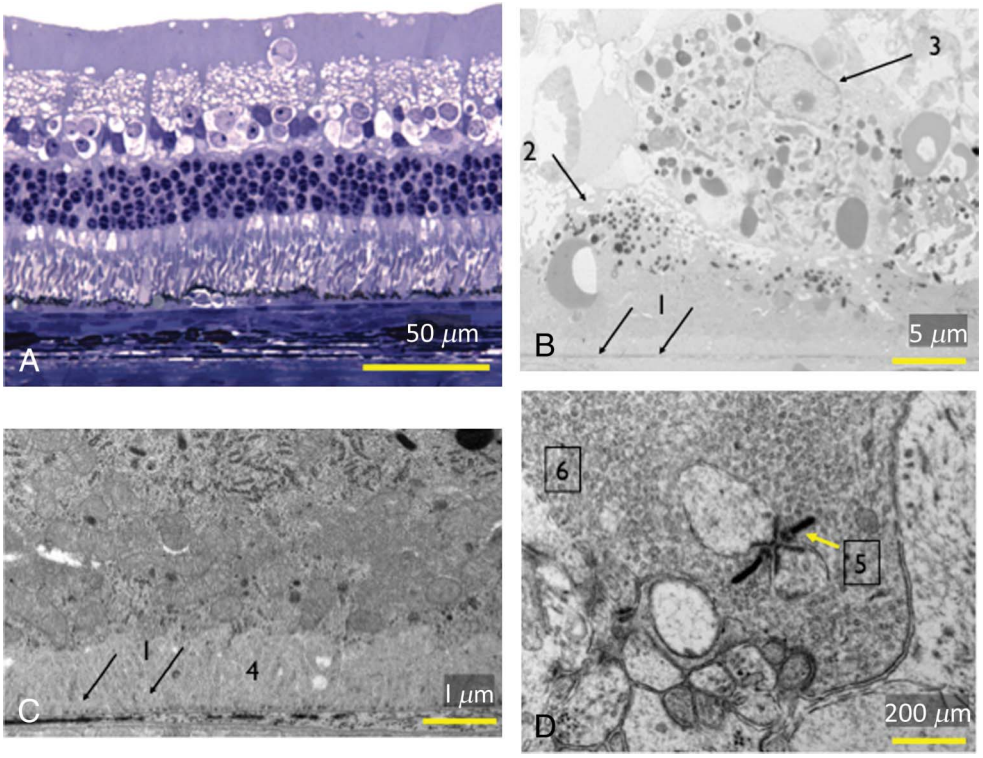

Fig. 8. A. Light microscopy of the 30% exposure with 200 μm spot size at 3 days does not show any visible damage. **B.** Transmission electron microscopy in the center of the exposure shows normal Bruch membrane (1), normal RPE cell (2), and an elevated RPE cell with phagosomes of the outer segments at the center of the laser spot (3). **C.** Higher magnification TEM shows presence of the normal RPE basal in-foldings (4) above Bruch membrane (1) at the center of the laser spot. **D.** Transmission electron microscopy of the outer plexiform layer in the treated area shows normal synapses between a photoreceptor and a bipolar cell, with synaptic ribbon (5) and vesicles (6).

COLOR

COLOR

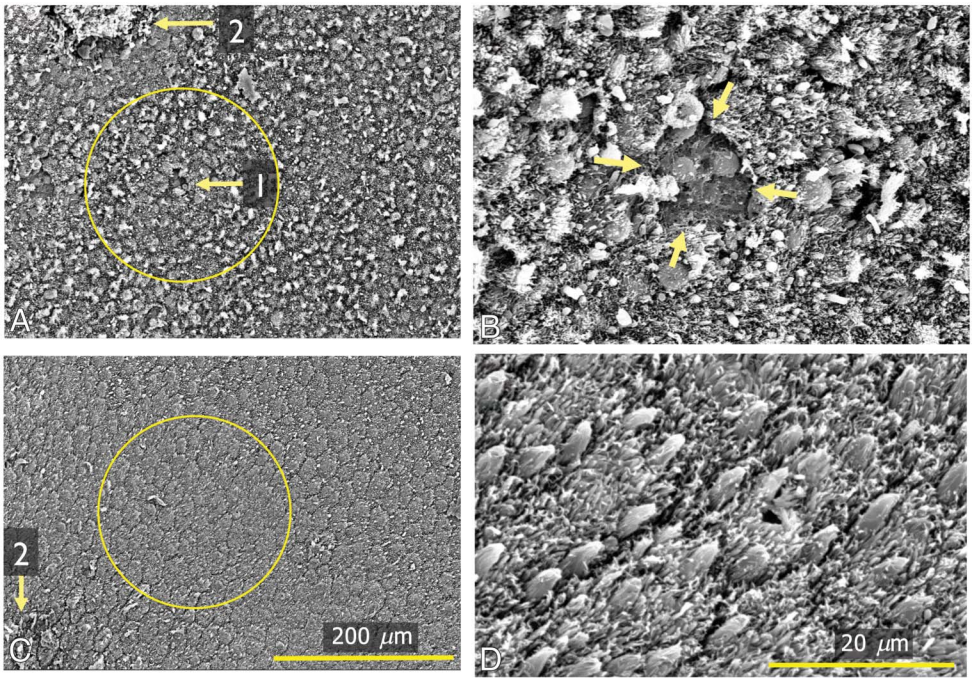

Fig. 9. A. Scanning electron microscopy of the RPE in the 30% exposure area at 1 day. The 200 μm laser spot is outlined by the yellow circle. Only 1 damaged cell (1) could be identified in the treatment area. An edge of the adjacent marker burn (2) can also be seen. **B.** Higher magnification view of the damaged RPE cell in the center of the laser exposure. **C.** After 7 days, there were no visible signs of damage to RPE layer inside the irradiated spot (circle). The marker burn (2) is still visible. **D.** Higher magnification view demonstrates normal RPE morphology in the treated area.

healing response of the RPE to thermal injury activates a cellular cascade, resulting in the therapeutic effects of the laser treatment in the nonproliferative macular diseases. Because this response is activated by the cells surviving the hyperthermal treatment, the goal would then be to maintain the temperature rise below the threshold of irreversible thermal damage.[13] The challenge with such sublethal treatment is the titration method and optimization of the laser parameters to provide reproducible results within the natural variability of pigmentation and transparency of the ocular tissues.

The EpM algorithm was designed to address this challenge by mapping computational model–based values of tissue damage (Arrhenius integral) to a linear scale of laser energy, relative to a visible titration level. Variability in retinal pigmentation and media transparency necessitates titration of the laser power for every patient. The titration algorithm described here for EpM begins with defining the laser power at 20 ms pulse duration to produce a barely visible burn within 3 seconds after the laser pulse. With this energy level defined as 100%, all other pulse energies are expressed as a percentage of this titration threshold. Light scattering and absorption are linear phenomena, and therefore, despite variability of the coagulation threshold from patient to patient, 50 or 30% setting on EpM will always correspond to half or a third of the titration threshold energy. Even though the thresholds for creating the barely visible lesion varied from rabbit to rabbit in this study by ~50% (70 to 110 mW), yet relative to the threshold in every animal, the results at the energy reduced by the same fraction were very reproducible.

Our study confirmed reproducibility of tissue effects when laser settings were applied based on the EpM algorithm and our titration protocol, ranging from very intense to very low settings. At 75% to 120% energy levels, the photoreceptors and RPE are selectively damaged, leaving the inner retina intact. These lesions heal over 2 months, reestablishing the photoreceptors layer and local synapses between migrated photoreceptors and preserved bipolar cells.[24] If the goal of photocoagulation for proliferative diabetic retinopathy is reduction of the number of photoreceptors to decrease metabolic rate and diminish expression of the angiogenic factors, this goal can be accomplished while avoiding the retinal scarring common to the more intense burns.

Because the settings 100% and higher provide ophthalmoscopically visible lesions, they allow immediate feedback regarding the changes in the laser uptake from one point to another. The main challenge is therefore in the lower settings, where intended tissue effects remain below the threshold for immediate clinical visibility. With consistent titration of the 100% level to the barely visible endpoint, we have shown reproducible tissue effects in subvisible lesions. At 50% to 75% energy levels, the damage was confined primarily to RPE, with minor effect on photoreceptors. This could offer the optimum range for a strategy involving a very limited photoreceptor

damage in the macula, like the modified Early Treatment Diabetic Retinopathy Study.[25] At these settings, the photoreceptors migrate from the adjacent areas and rapidly restore continuity of the outer retina, leaving no scarring behind.

Subvisible photostimulation has been tested in several clinical trials for DME and other retinal diseases with near-infrared micropulse laser.[13] One of the major difficulties in subvisible laser therapy is the risk of undertreatment. We previously determined that enhanced expression of the heat shock protein (HSP-70) in the retina begins at laser power approximately half of the RPE damage threshold.[17] That study, and correlation of the computational model with clinical data,[18] revealed that Arrhenius integral Ω in the subvisible macular therapy was in the range of 0.1 to 1. These data were used for calibration of the computational model underlying the EpM algorithm. With our titration protocol, tissue damage at 30% energy level was limited to a single RPE cell in the center of the 200-μm spot. Although modeling of the laser–retina interaction is inherently limited by the imprecise knowledge of light absorption, heat conduction and cellular damage model parameters, the utility of such modeling is supported by this observation. Two different laser modalities (577 nm, $<$10 ms pulse, and near-infrared micropulse) resulted in the same observable effect for the same Arrehnius integral range: laser effects below the Arrhenius integral of 1 are nondestructive.

In recent years, intravitreal injections of anti-angiogenic agents have been effectively used to treat DME.[25] However, frequent injections are burdensome for patients and physicians, are associated with very high cost to the healthcare system, and carry cumulative risk of ocular infection with potentially devastating consequences. The combination of a rapid response to intravitreal anti–vascular endothelial growth factor therapy and a long-lasting effect of nondestructive laser therapy might decrease the need of frequent injections and thereby improve patient care. Although recent results comparing prompt and deferred laser therapy in conjunction with anti–vascular endothelial growth factor pharmacological treatments favored deferring laser based on visual acuity results,[25] optimization of the laser treatment protocols toward less damaging or nondamaging strategies while increasing spot density might provide more effective alternative to classic coagulation for DME therapy. This hypothesis remains to be tested in clinical trials.

Visibility of the retinal lesions is subjective; it may depend on transparency of the ocular media, tissue health, and other complicating factors and tends to change over time. To reduce the level of subjectivity, we used a binary criterion in titration: whether the lesion is visible or not, rather than the traditional (and more subjective) scale of "light," "moderate," and "intense" clinical grades in titration. To minimize the factor of lesion evolution over time, visibility was defined as immediate, that is, within 3 seconds after the laser pulse. This method provided consistent results based on comparison with histologic analysis and SEM. Moreover, implementation of the EpM protocol on pattern-scanning laser systems allows maintaining some spots in the grid at 100% (or above) to mark locations of the subvisble treatment and to provide an immediately visible reference, allowing for power adjustment to maintain the same ophthalmoscopic visibility grade throughout the fundus.

In conclusion, the EpM algorithm and associated titration protocol provide an approach to reproducible subvisible retinal laser therapy. Clinical trials are necessary to verify the ranges of visibility of the retinal damage in humans, and to test the reproducibility, efficacy, and safety of subvisible treatment parameters in various retinal diseases.

Key words: laser photocoagulation, imaging, photostimulation, computational model.

References

1. Blumenkranz MS, Yellachich D, Andersen DE, et al. Semiautomated patterned scanning laser for retinal photocoagulation. Retina 2006;26:370–376.
2. Al-Hussainy S, Dodson PM, Gibson JM. Pain response and follow-up of patients undergoing panretinal laser photocoagulation with reduced exposure times. Eye (Lond) 2008;22:96–99.
3. Roider J, Hillenkamp F, Flotte T, Birngruber R. Microphotocoagulation—selective effects of repetitive short laser-pulses. Proc Natl Acad Sci U S A 1993;90:8643–8647.
4. Bandello F, Brancato R, Menchini U, et al. Light panretinal photocoagulation (LPRP) versus classic panretinal photocoagulation (CPRP) in proliferative diabetic retinopathy. Semin Ophthalmol 2001;16:12–18.
5. Cardillo JA, Dare AJ, Peroni R, et al. Treatment optimization for short pulsed and low energy delivery of pascal modified macular grid laser photocoagulation for diabetic macular edema. Invest Ophthalmol Vis Sci 2011;52:591.
6. Paulus YM, Jain A, Gariano RF, et al. Healing of retinal photocoagulation lesions. Invest Ophthalmol Vis Sci 2008; 49:5540–5545.
7. Framme C, Schuele G, Roider J, et al. Influence of pulse duration and pulse number in selective RPE laser treatment. Lasers Surg Med 2004;34:206–215.
8. Roider J, Michaud NA, Flotte TJ, Birngruber R. Response of the retinal pigment epithelium to selective photocoagulation. Arch Ophthalmol 1992;110:1786–1792.
9. Roider J, Liew SH, Klatt C, et al. Selective retina therapy (SRT) for clinically significant diabetic macular edema. Graefes Arch Clin Exp Ophthalmol 2010;248:1263–1272.
10. Lavinsky D, Cardillo JA, Melo LA, et al. Randomized clinical trial evaluating mETDRS versus normal or high-density micropulse photocoagulation for diabetic macular edema. Invest Ophthalmol Vis Sci 2011;52:4314–4323.

11. Figueira J, Khan J, Nunes S, et al. Prospective randomised controlled trial comparing sub-threshold micropulse diode laser photocoagulation and conventional green laser for clinically significant diabetic macular oedema. Br J Ophthalmol 2009; 93:1341–1344.
12. Venkatesh P, Venkatesh P, Ramanjulu R, et al. Subthreshold micropulse diode laser and double frequency neodymium: YAG laser in treatment of diabetic macular edema: a prospective, randomized study using multifocal electroretinography. Photomed Laser Surg 2011;29:727–733.
13. Sivaprasad S, Elagouz M, McHugh D, et al. Micropulsed diode laser therapy: evolution and clinical applications. Surv Ophthalmol 2010;55:516–530.
14. Sramek C, Paulus Y, Nomoto H, et al. Dynamics of retinal photocoagulation and rupture. J Biomed Opt 2009;14:034007.
15. Birngruber R, Hillenkamp F, Gabel VP. Theoretical investigations of laser thermal retinal injury. Health Phys 1985;48:781–796.
16. Schuele G, Rumohr M, Huettmann G, Brinkmann R. RPE damage thresholds and mechanisms for laser exposure in the microsecond-to-millisecond time regimen. Invest Ophthalmol Vis Sci 2005;46:714–719.
17. Sramek C, Mackanos M, Spitler R, et al. Non-damaging retinal phototherapy: dynamic range of heat shock protein expression. Invest Ophthalmol Vis Sci 2011;52:1780–1787.
18. Luttrull JK, Sramek C, Palanker D, et al. Long-term safety, high-resolution imaging, and tissue temperature modeling of subvisible diode micropulse photocoagulation for retinovascular macular edema. Retina 2012;32:375–386.
19. Arjamaa O, Nikinmaa M. Oxygen-dependent diseases in the retina: role of hypoxia-inducible factors. Exp Eye Res 2006;83: 473–483.
20. Klein R, Klein BE, Knudtson MD, et al. Systemic markers of inflammation, endothelial dysfunction, and age-related maculopathy. Am J Ophthalmol 2005;140:35–44.
21. Stefánsson E. The therapeutic effects of retinal laser treatment and vitrectomy. A theory based on oxygen and vascular physiology. Acta Ophthalmol Scand 2001;79:435–440.
22. Schatz H, Madeira D, McDonald HR, Johnson RN. Progressive enlargement of laser scars following grid laser photocoagulation for diffuse diabetic macular edema. Arch Ophthalmol 1991;109:1549–1551.
23. Muqit MM, Denniss J, Nourrit V, et al. Spatial and spectral imaging of retinal laser photocoagulation burns. Invest Ophthalmol Vis Sci 2011;52:994–1002.
24. Jones BW, Huie P, Wang H, et al. Neural activity in the inner retina after photocoagulation. Invest Ophthalmol Vis Sci 2011; 52:1170.
25. Diabetic Retinopathy Clinical Research Network; Elman MJ, Qin H, Aiello LP, et al. Intravitreal ranibizumab for diabetic macular edema with prompt versus deferred laser treatment: three-year randomized trial results. Ophthalmology 2012;119: 2312–2318.